International Journal of Multiphase Flow 36 (2010) 940–949

Contents lists available at ScienceDirect

International Journal of Multiphase Flow

journal homepage: www.elsevier.com/locate/ijmulflow

Experimental study of jet structure and pressurisation upon liquid nitrogen injection into water

H. Clarke, A. Martinez-Herasme, R. Crookes, D.S. Wen *

School of Engineering and Materials Science, Queen Mary University of London, Mile End Road, London E1 4NS, UK

ARTICLE INFO

Article history:
Received 17 December 2009
Received in revised form 9 June 2010
Accepted 30 July 2010
Available online 8 August 2010

Keywords:
Cryogenic engine
Boiling
Liquid nitrogen
Fuel–coolant interaction
Zero-emission vehicle

ABSTRACT

The rapid phase change and heat transfer obtained by direct contact heat exchange between a cryogen and water can generate high rates of pressurisation, which is of interest to a number of applications. A visualization study of liquid nitrogen injection into water is conducted in this work, with synchronized pressure and temperature measurement, to obtain insight into this complex phenomenon. High speed imaging reveals a four-stage evolution of liquid nitrogen jet structure upon injection into water, with a thick vapour blanket forming around a liquid nitrogen core and break-up brought on predominantly through impact with the vessel wall. Maximum pressurisation rate occurs in the third stage of injection due to a combination of heat and mass transfer. Pressurisation rates in excess of 350 bar/s are recorded and found to vary proportionally with injection pressure. The scenario of gaseous nitrogen injection is also investigated, and compared with liquid nitrogen injection. A clear advantage of liquid nitrogen injection is elucidated from the point of heat transfer and pressurisation, and implications for use in a cryogenic engine are discussed.

1. Introduction

Direct contact heat exchange between two fluids with different temperatures occurs in many industrial and natural processes. The large interfacial area between two interpenetrating mass streams allows rapid heat exchange. Phase change may occur in one or both streams, which can enhance the mixing process even to the extent of potentially violent vapour explosions (Khabeev, 1999). This is of some concern for safety analyses in the nuclear industry and for storage and transport of cryogenic fluids such as liquefied natural gas. Fuel–coolant interactions (FCI) for example, can occur during the course of an accident in a light water reactor, where high temperature molten metal is in contact with an ambient temperature coolant, resulting in film boiling of the coolant fluid around the jet and subsequent fragmentation of the melt (Dinh et al., 1998). However such a rapid heat and mass transfer process is not always deleterious. The concept of rapid boiling and expansion of a cryogen, such as liquid air, in a warmant fluid has been proposed for the development of a zero-emission cryogenic engine (Clarke et al., 2009; Ordonez et al., 2001). The concept relies on a controlled injection of cryogen into a pool of warm liquid, in a similar way to FCIs, to induce a heat transfer process that results in a rapid internal pressure increase.

Few experimental studies have been conducted for the injection of cryogen into water. Dahlsveen et al. (2001) investigated such a process for accident analysis in the transportation of liquefied natural gas. With the phase change occurring in the injected medium, experiments showed a much thicker vapour blanket and larger jet spreading angle. Wen et al. (2006a) conducted a number of injections of liquid nitrogen into water to establish heat transfer and pressurisation rates for application to a cryogenic engine. Using a large enough pressure vessel to neglect changes in free volume space, pressurisation rates of up to 5 bar/s were recorded but without observation of the break-up dynamics. Injection was from the saturation temperature and therefore unavoidably in the multiphase region, and detailed information as to the thermodynamic state of pre-injection was not available. Heat transfer coefficients approximated for the latent heat transfer with assumed surface area were comparable to values found in other works on boiling heat transfer over very rough surfaces.

Conversely, the injection of water into a cryogen pool has been studied as a cost effective substitute to full scale FCI tests. A series of experiments were aimed at determining the conditions under which a vapour explosion might take place, involving injection at different pressures and volumetric ratios of water/nitrogen (Archakositt et al., 2004). Given the large free volume of the pressure vessel, rates of pressure rise were impressively high at 25 bar/s. These were an order of magnitude greater than those recorded when vapour explosion did not occur, and with generally less than half the inception time.

* Corresponding author. Tel.: +44 20 78823232; fax: +44 20 89831007.
E-mail address: d.wen@qmul.ac.uk (D.S. Wen).

0301-9322/$ - see front matter © 2010 Elsevier Ltd. All rights reserved.
doi:10.1016/j.ijmultiphaseflow.2010.07.005

Some numerical studies have been conducted to understand the two-fluid injection process. An attempt to analyse the thermodynamics of similar experiments using the MELCOR systems code was made with a view to accident analysis for cryogenically cooled magnets (Duckworth et al., 2000). This was not a simulation of the injection, but a method to calculate the interfacial area from experimental pressure curves, based on an established empirical heat transfer coefficient for film boiling over a vertical surface. The results are of limited wider use however, due to a lack of observation of the structure of the water–nitrogen interface on injection. In particular this makes it difficult to verify the suitability of the heat transfer coefficient correlation. The analysis was also limited to have constant surface area and temperature, obliging a fudge to be performed in which the heat transfer coefficient is linearly reduced to zero at a pre-determined time to allow convergence to equilibrium. For a simplified incompressible and isothermal case, a numerical code written along similar lines to MELT-3D (Nourgaliev et al., 2003), a Lagrangian FCI code, was developed allowing the injection structure to be approximately simulated (Dahlsveen et al., 2001). It is unclear however, to what extent pressure curves could be predicted for injection into a closed vessel or with the inclusion of sensible heat transfer.

To advance our understanding of this injection process, a visualization study of liquid nitrogen injection into water is conducted in this work. A small vessel volume, relative to previous experiments (Wen et al., 2006a), is used to more accurately reflect the confined scale of injection into a reciprocating engine cylinder. Careful design allows the thermo-physical state of the pre-injection nitrogen to be known, i.e. pure liquid nitrogen vs. vapour–liquid mixture. Through the use of high speed imaging equipment, the break-up of the nitrogen jet is characterised, with a view to establishing the most appropriate modelling solution for the process. Pressure and temperature profiles are obtained and synchronized with images in an attempt to obtain insight into the complex heat transfer mechanisms involved. The effect of injection pressure on the pressurisation rate and jet dynamics are investigated, as are the implications of these results on the cryogenic engine performance.

2. Experimental setup

The experimental rig (Fig. 1) consists of a single shot injector, a cooling system, and a small pressure vessel with viewing windows so that high speed imaging of the injection process is possible.

Nitrogen is delivered through an insulated hose from a high pressure Dewar, in liquid or gas phase at up to 16 bar. A manual valve allows the feed line to be purged before testing, cooling the hose and delivering a fresh charge of nitrogen to the inlet. A pressure transducer and thermocouple feed-through seal are mounted upstream of the injector. A T-type thermocouple runs through the compressed Teflon seal and down the cooling pipe to a point just upstream of the valve. Thus the thermodynamic state of the nitrogen may be known prior to injection, providing it is of single phase.

The injector is made of a 50 mm length of aluminium alloy pipe with an inside diameter of 8 mm. The opening and close of the injection is controlled by an off-the-shelf, seat type cryogenic solenoid valve. Both pipe and valve are built into a cooling bath so that the nitrogen can be subcooled to the desired temperature prior to injection. A secondary flow of liquid nitrogen at lower pressure is used as the cooling fluid. A valve at the bath exit is used to manually regulate this secondary flow, allowing some control over the cooling rate. An identical cryogenic solenoid valve is placed between the injector and pressure vessel, orientated to operate in the opposite direction to the flow. Upon injection it is opened simultaneously with the primary solenoid valve and prevents leakage upstream if the post injection vessel pressure exceeds the feed pressure.

The pressure vessel is an aluminium alloy cylinder of radius 65 mm and depth 40 mm with Perspex windows clamped onto each end. A rapid response quartz crystal pressure transducer and two T-type thermocouples are used to measure the pressure and temperatures within the vessel. These thermocouples are positioned to be above and below the waterline under quiescent conditions, measuring gas and water temperatures respectively. Ball valves in the bottom and side of the vessel are opened to allow water to be pumped through the vessel, preventing misleading measurements caused by a temperature gradient developing in the water as the nitrogen is subcooled pre-injection. These are shut-off manually immediately prior to injection. A relief valve is fitted to the vessel to prevent pressurisation above 30 bar.

Between tests, water is circulated through the vessel to re-heat it to ambient temperature. Warm nitrogen gas is also circulated through the injector assembly to remove moisture which can cause the valves to freeze in subsequent experiments.

A high speed camera positioned at one end of the vessel is used for imaging at rates up to 8000 frames per second. A powerful steady state light source equipped with a diffuser is positioned at the opposite end. A low power light source is directed through the front viewing window via fibre optics. The camera is triggered by the leading edge of a 5 V pulse generated within the LabVIEW program, initiated by the operator. The same pulse triggers a solid state relay switch which powers up the solenoid valves, hence synchronising the data acquisition with the image acquisition. The period of injection is dependent on the trigger pulse width, which is set manually within the program. However valve closing is driven by the valve springs and pressure gradients, making determination of the exact closing time difficult. All run data is acquired and stored through National Instruments Data-Acquisition hardware and LabVIEW, at a rate of 1000 samples per second.

3. Results and discussion

By controlling the secondary liquid nitrogen flow around the cooling bath, different thermodynamic states of nitrogen prior to injection can be established. A number of nitrogen injections are conducted, of gaseous or liquid phase, into a pool of either ambient water or air. All experiments involve injection vertically downwards through a 2 mm diameter nozzle with L/D ratio of 5. The parameters for each test are shown in Table 1. Where injection is into water, a volume of approximately 90 ml is used, leaving 50 ml free volume in the vessel.

3.1. Liquid nitrogen injection into water

In the injection run 3 liquid nitrogen is injected into water at a feed pressure of ~7 bar and with a temperature just below saturation. The vessel pressure is shown in Fig. 2a over a 6 s timescale and additionally in Fig. 2b for the first 300 ms only. Data is aligned so that time 0 s corresponds to the trigger signal, with mass injection beginning about 10 ms later. Initially, pressurisation is extremely rapid at ~190 bar/s up to 6 bar. At this point the pressure profile rounds off smoothly, to a plateau of ~14 bar some 5 s after injection.

Temperature profiles for the gaseous and liquid volumes in the vessel are shown in Fig. 3. The pre-injection gas temperature is a few degrees below that of the water, as the air volume is cooled by inadvertent conduction through the apparatus to the liquid nitrogen bath as the feed nitrogen is cooled. On injection the temperature rises briefly, as the thermocouple comes into contact with the warmer water during the turbulent mixing process that

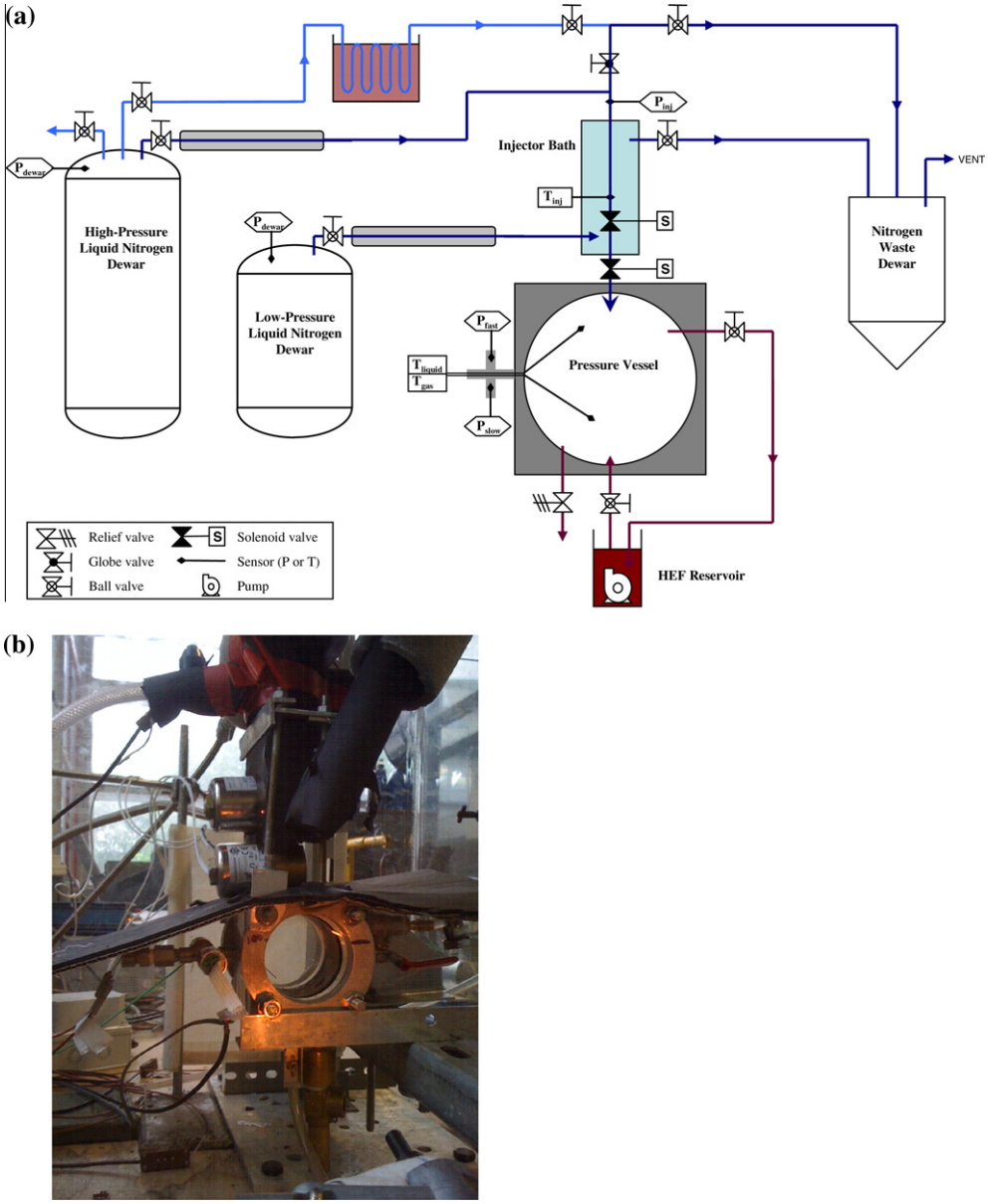

Fig. 1. Nitrogen injection setup and apparatus: (a) schematic of experimental rig; (b) picture of injectors and pressure vessel.

Table 1
Injection run parameters.

Run	Injection phase	Pressure/bar	Temperature/K	Mass N_2/g	Mass water/g
1	Gaseous	7.00	273.7	0.105	100.9
2	Gaseous	6.92	273.3	0.295	100.2
3	Liquid	6.51	99.3	0.750	96.2
4	Gaseous	6.81	149.7	0.135	92.2
5	Liquid	6.73	94.2	0.856	90.4
6	Gaseous	6.93	150.3	0.138	93.7
7	Liquid	8.92	96.4	0.839	91.2
8	Liquid	14.09	101.2	1.158	85.6
9	Liquid	14.06	101.4	1.445	0
10	Liquid	14.13	106.9	1.349	0
11	Liquid	14.21	101.3	1.390	0

follows. Gas temperature falls about 10 K before rising to a plateau. This relatively low drop in temperature as cold nitrogen is added is a consequence of the majority of heat transfer occurring before liquid and gas volumes in the vessel have separated. At less than

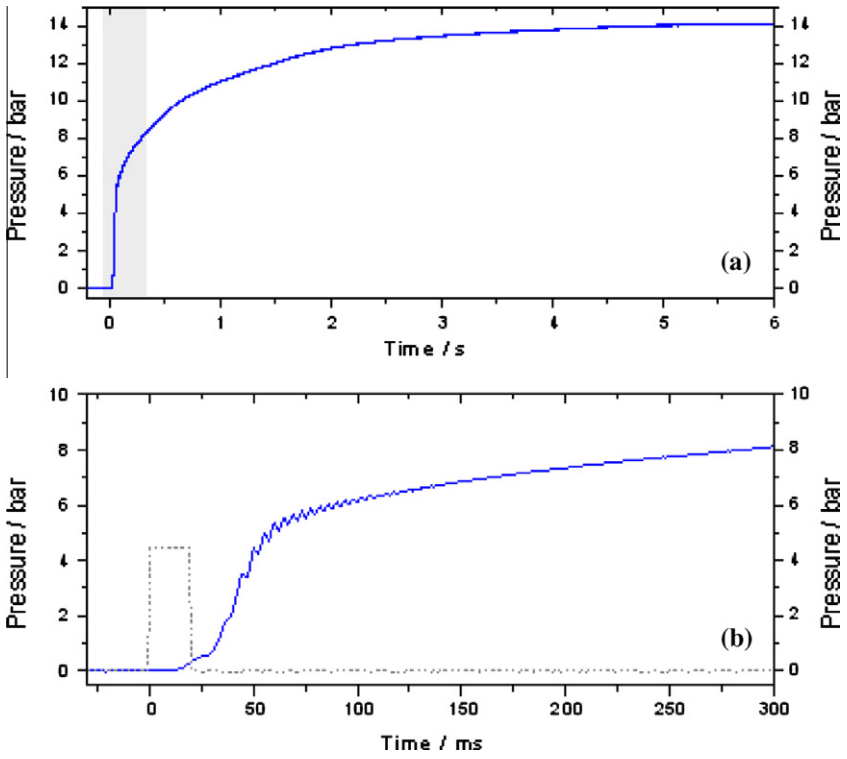

Fig. 2. Vessel pressure for liquid nitrogen injection into water (run 3). Shown over 6 s (a) and enlarged in (b) over the 300 ms timescale identified by the shaded region. The dotted line shows the trigger signal at time = 0.

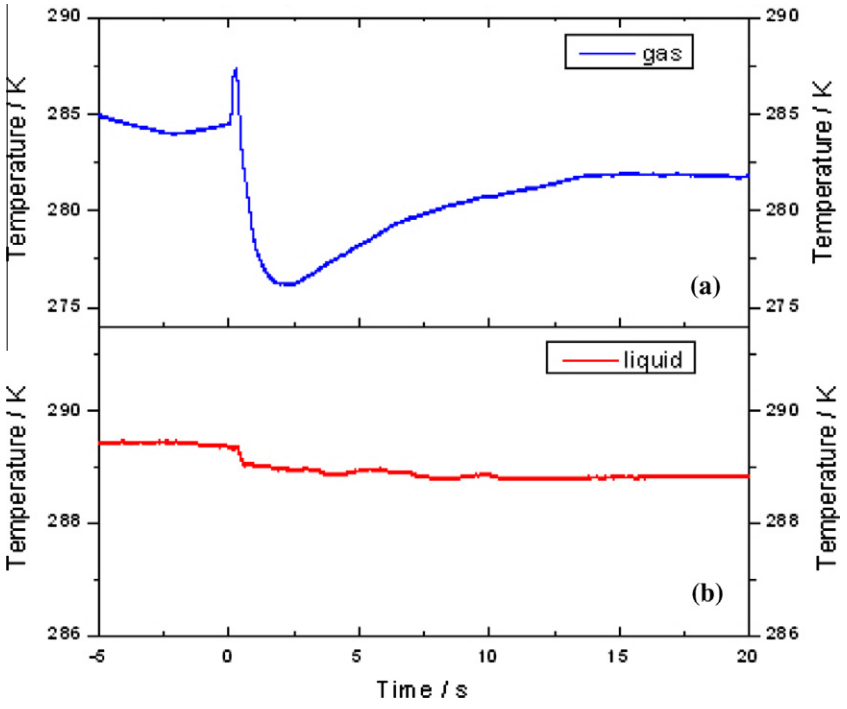

Fig. 3. Temperature profiles for liquid nitrogen injection into water (run 3). Shown over a 25 s timescale for the gaseous (a) and liquid volumes (b) of the pressure vessel.

0.5 K, the drop in water temperature over the injection is low due to the large ratio of water to nitrogen mass involved in the process.

The image sequence for injection run 3 is displayed in Fig. 4, with the elapsed time from the trigger signal and vessel pressure given below each image. By 30 ms, the presence of a liquid phase core is noticeable, surrounded by a thick vapour blanket as characterised in earlier studies (Dahlsveen et al., 2001; Harstad, 1992), and from this point the rate of pressurisation accelerates. However these early studies were more concerned with the behaviour of the jet in quasi-steady state.

From these images the injection and break-up can be characterised in four stages:

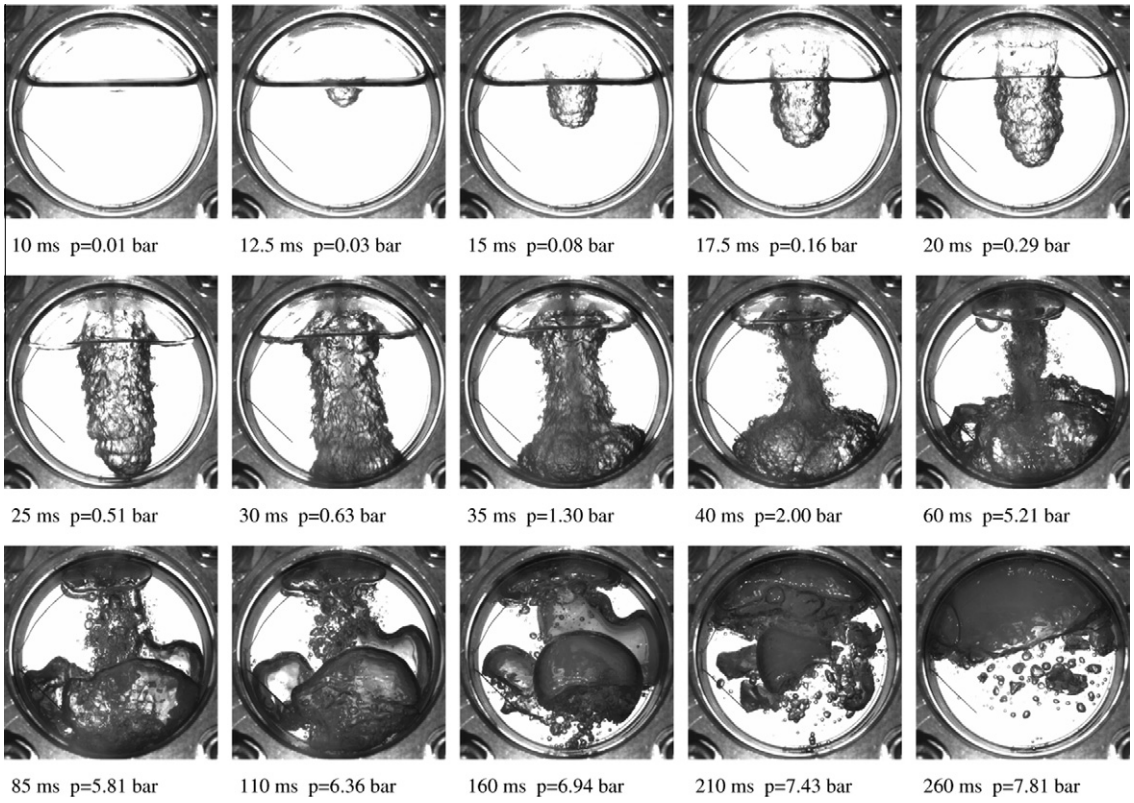

Fig. 4. High speed images of the liquid injection into water (run 3). Time from injection trigger signal, and vessel pressure are given below each image.

(1) Gaseous pre-injection stage: liquid nitrogen flashes as it exits the nozzle and the column of nitrogen gas impinges on and propagates through the water pool.
(2) Liquid injection: the liquid begins to be injected into the void created by the nitrogen gas. The jet sets up a liquid core within a blanket of its own vapour. A velocity gradient forms across the vapour blanket due to viscous effects, as the water on the outside is almost static, while the liquid nitrogen on the inside is moving at a higher speed. Despite this there is still no significant break-up into droplets from the vapour blanket into the water, although the formation of ligaments due to Kelvin–Helmholtz instability is observed.
(3) Impact with the opposing wall: upon impact the jet widens and is deflected, filling the bottom part of the vessel. The top half of the jet narrows as pressure increases, and begins to break-up, forming ligaments and bubbles as the injection finishes. The break-up here is caused mainly by inertial impact rather than by Kelvin–Helmholtz instability and fragmentation as we might expect to see in a larger vessel.
(4) Buoyancy driven break-up: the nitrogen in the bottom half of the vessel breaks up into large, and then smaller bubbles as buoyancy forces take over and drive the nitrogen upwards.

These four stages are marked on the pressure profile in Fig. 5 for clarity. Stages (1) and (2) are short transient stages, in which the jet is established and pressure rise is low, whereas stage (3) is associated with the rapid pressure rise and is more steady state. Based on the image sequences, and order of magnitude calculations for valve open time, the injection is thought to end at the 'corner' of the pressure curve, shortly before the end of stage (3). The very high initial pressurisation rate is thus a result of both mass transfer of nitrogen into the free volume and heat transfer to the nitrogen.

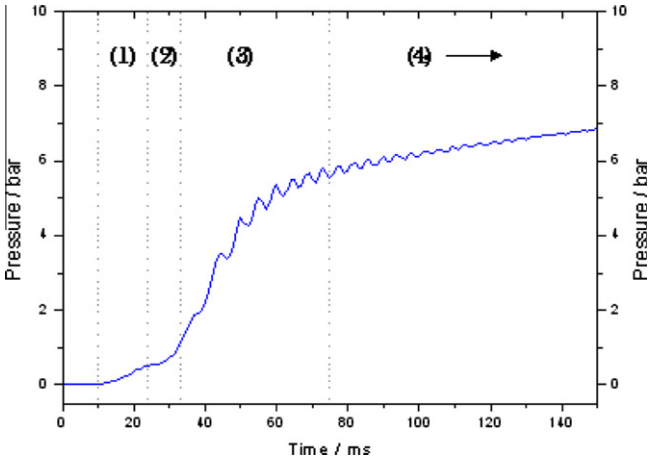

Fig. 5. Pressure curve correspondent to images of injection run 3, with the four stages of jet evolution marked.

Some degree of this heat transfer results from the contact between the nitrogen jet and vessel wall as observed in stage (3). However, this is likely to be small relative to heat transfer from the water due to the large heat transfer coefficient between liquid nitrogen and water, and far greater area of the irregular and turbulent water–nitrogen interface. Stage (4) is also associated with a large pressure increase, based solely on heat transfer, but over a much longer timeframe.

It is not possible to closely observe the behaviour of the liquid core in these experiments, as this part of the injection is obscured by the uneven liquid–gas interface. This liquid behaviour is however vital to fully understanding the steady stage (3) of this injection. One possible method for studying the core is to reduce the

depth of the pressure vessel sufficiently so that the jet is sandwiched between the two Perspex plates, allowing the jet to be viewed as a cross-section. This seems to have been a successful technique in some other works where interface propagation has been studied (Reinke and Yadigaroglu, 2001), although it is possible that some of the 3D effects may be lost, changing the overall behaviour of the jet.

Liquid nitrogen is injected at pressures of 7, 9 and 14 bar to allow comparison of pressurisation rates. The different injection temperatures (Table 2: runs 5, 7 and 8) reflect similar degrees of subcooling below the saturation point, which is a function of pressure. The level of subcooling is quantified here as the ratio of injection temperature to saturation temperature, and is held constant at $T_{inj}/T_{sat} \sim 0.93$ for these injections. Pressure profiles are shown as a ratio of local pressure to the peak pressure (Fig. 6) to highlight the speed with which maximum pressure is approached. Because the peak pressure is approximately proportional to the injected mass, this allows comparison of pressurisation of the inherently different masses injected at different pressures for a fixed nozzle size and vessel volume. Gradients taken from three sections (Fig. 7) during, immediately after injection, and prior to plateau are shown in Table 2. While the rate during the injection is bound to be greater for higher injection pressure due to higher mass flow, it is clear that enhanced heat transfer continues post injection. The gradients nearer to the plateau level show lower rates for the higher injection pressures, suggesting that temperature equilibrium is reached more rapidly. This is also evident from Fig. 6, and simply shows that a larger proportion of the energy transfer occurs near the beginning of the pressurisation, due to a higher heat transfer coefficient.

These rates of pressurisation during the liquid injection are extremely high. In similar injection tests of cryogen into water (Wen et al., 2006a) with larger free volume, far lower rates of the order of 5 bar/s were observed. Plotting all the injection gradients, adjusted for marginal differences in the vessel free volume (90 ml water volume is used ±8% in all runs), against injection pressure (Fig. 8), a linear fit is seen. Interpolation for the injection pressure of 3.5 bar used by Wen et al. gives a pressurisation rate of 53 bar/s: the factor of 10 difference is about what we would expect from the difference in free volume space between the experiments.

3.2. Gaseous nitrogen injection into water

The rapid boiling of injected liquid nitrogen is expected to increase interfacial area and dramatically enhance the heat transfer rate between the cryogen and water, resulting in an increased pressure time derivative. The extent to which this occurs can be seen in Figs. 9 and 10, showing data from injection runs 1, 5 and 6. Run 1 is the injection of nitrogen at atmospheric temperature, thus without major heat transfer. Run 5 is liquid nitrogen injection with the associated boiling heat transfer. Run 6 is the injection of cold gaseous nitrogen at 150 K, involving sensible heat transfer only. Out of necessity liquid nitrogen injection must occur below the saturation point (i.e. in the subcooled state) and cold gaseous injection at a temperature above which no multiphase behaviour is observed in the injectors. High speed images for injection run

Table 2
Comparison of pressure increase rates.

Injection pressure/bar	Pressure time derivative/bar/s		
	Section 1	Section 2	Section 3
14	367	23.6	1.14
9	213	13.3	1.72
7	173	8.7	1.82

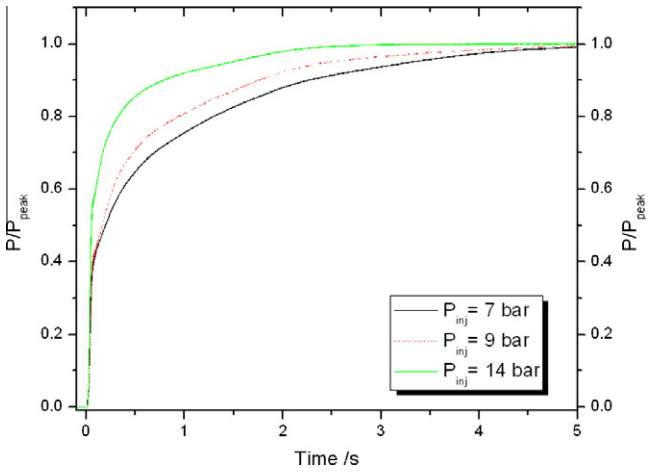

Fig. 6. Liquid nitrogen injection at different pressures into water. Profiles of pressure as a ratio of peak pressure displayed for injections at 7, 9 and 14 bar (runs 5, 7 and 8 respectively).

6 are shown in Fig. 11. The gaseous nitrogen jet clearly propagates through the water pool more rapidly than the liquid jet during stage (1): a higher injection velocity is expected due to lower density and higher compressibility. This causes a quicker initial pressure rise in the gaseous injection. Subsequently a larger spreading angle of the jet can be seen in the 30 ms image, and better mixing of liquid–gas phases 100 ms post injection.

The gaseous injections have a very different pressure profile to liquid injections. After the initial rise the pressure profile flattens sharply at the 50 ms mark, where the injection valves are assumed to close, and remains constant. This plateau level is much lower than that of liquid injection: mass transfer is reduced since the lower fluid density results in lesser mass flow rate through the nozzle for a given pressure ratio. Interestingly, there is only a minor difference between the injection profiles of gas at 150 K and at 274 K. This is probably due to the slightly larger free volume in run 6; with the same water level the difference would be more pronounced. It is clear that nearly all heat transfer occurs during the injection stage as there is no pressurisation after the valve shut-off.

Pressure time derivatives measured using a line of best fit are ~76 bar/s for gaseous injection, and more than double that for liquid injection at ~190 bar/s. Because of the difference in injection temperature driving the heat transfer of ~50 K, this is not an entirely fair comparison. Assuming that the pressure time derivative is proportional to the rate of heat transfer, which is calculated by Eq. (1), it is more appropriate to compare the values of the product $1/\Delta T\ dp/dt$. This is then proportional to the product of the heat transfer coefficient, h and interfacial area, A. This gives values of 0.97 and 0.54 bar/s K for liquid and gas injections respectively. The heat transfer enhancement from the boiling process is only 79% by this measure. Such a low increase may be due to the boiling of the injected nitrogen within a blanket of its own vapour, rather than by direct contact with the water, as noted previously.

$$\frac{dp}{dt} \propto \frac{dQ}{dt} = hA\Delta T \tag{1}$$

The benefit of using water as a heat transfer fluid is elucidated by comparison of injection runs 8 and 9. Liquid nitrogen is injected at 14 bar into water and gas respectively (Fig. 12). Injection into ambient gas utilises the whole vessel as free volume (140 ml) whereas the vessel is filled with 86 ml of water for run 8, leaving 54 ml free volume. The free volume into which the nitrogen expands affects the final pressure and rate of pressurisation for a given injection mass. It will also affect the injected mass as the

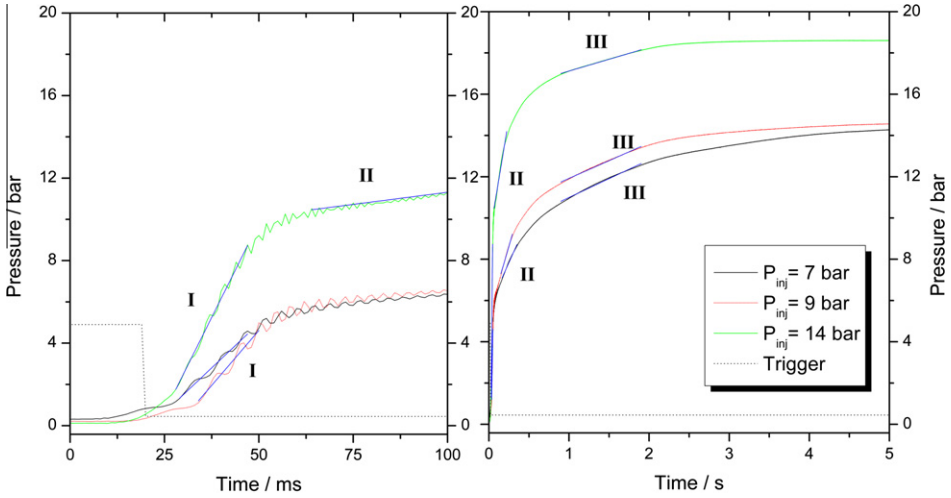

Fig. 7. Position of pressure time derivative calculation for sections I (left), II and III (right).

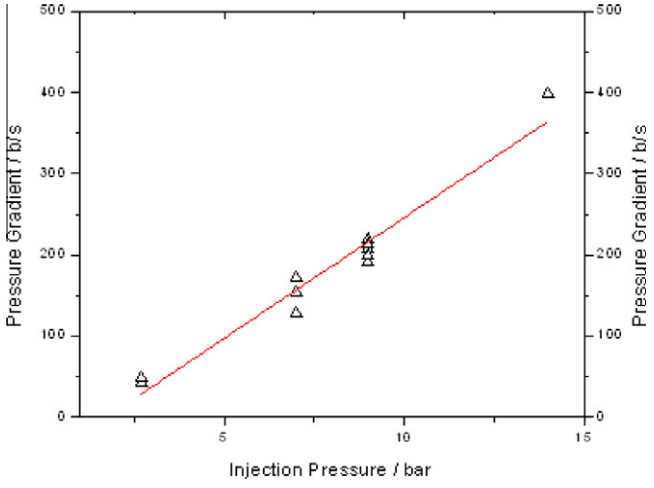

Fig. 8. Pressurisation rate dependence on injection pressure.

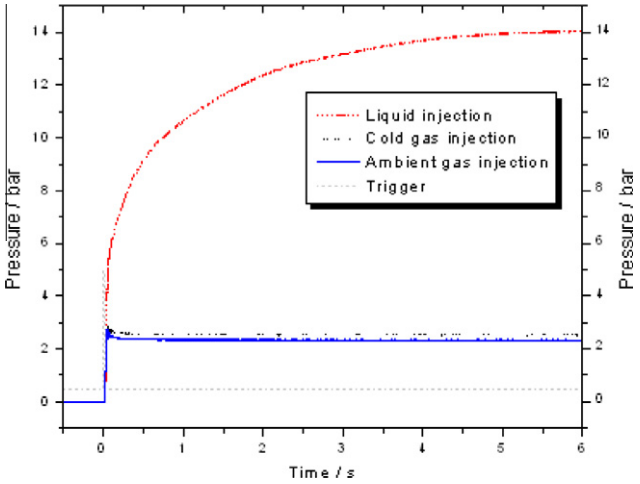

Fig. 9. Liquid, cold gaseous and ambient nitrogen injection shown over a 6 s timescale.

pressure differential across the solenoid valves drives the mass flow and affects the closing time. To compare these injections, the pressure values are normalised by peak pressure, which is

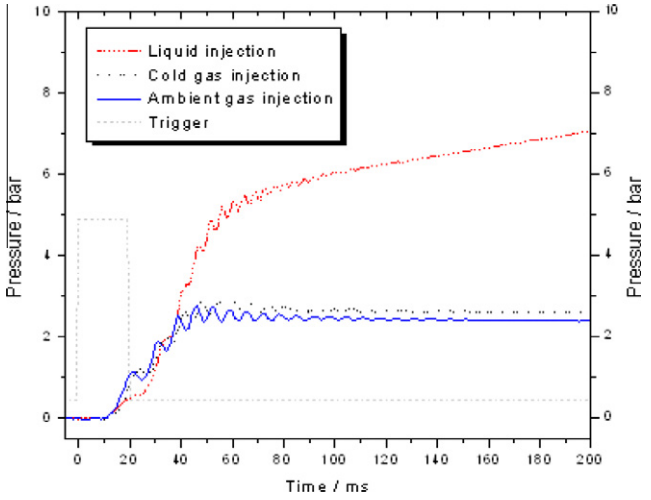

Fig. 10. Liquid, cold gaseous and ambient nitrogen injection shown over the first 200 ms after the trigger signal.

approximately linear with injected mass/free volume. With pressure time derivatives of 367 and 52 bar/s respectively, the rate at which peak pressure is approached during injection is 3.3 times higher with water than with gas. Immediately post injection this factor is reduced to 1.5.

3.3. Heat transfer analysis

The dual requirements on temperature measurement apparatus of sturdiness and fast response make quantification of heat transfer during the injection difficult. The multi-constituent nature of the process obscures temperature measurement further. However as a first-step analysis, steady-state pressure and temperature readings pre- and post injection allow some estimation of the heat transfer involved. Considering the injection process to involve the interaction of three closed systems, where system A comprises of the injected nitrogen, system B the ambient nitrogen in the vessel prior to injection, and system C the water in the vessel, the energy balance can be written from the first law as the following equation.

$$\begin{aligned} U_A^2 - U_A^1 &= Q_{B-A} + Q_{C-A} + Q_{other} - W_{A-B} - W_{A-C} \\ U_B^2 - U_B^1 &= -Q_{B-A} + Q_{C-B} + W_{A-B} - W_{B-C} \\ U_C^2 - U_C^1 &= -Q_{C-A} - Q_{C-B} + W_{A-C} + W_{B-C} \end{aligned} \quad (2)$$

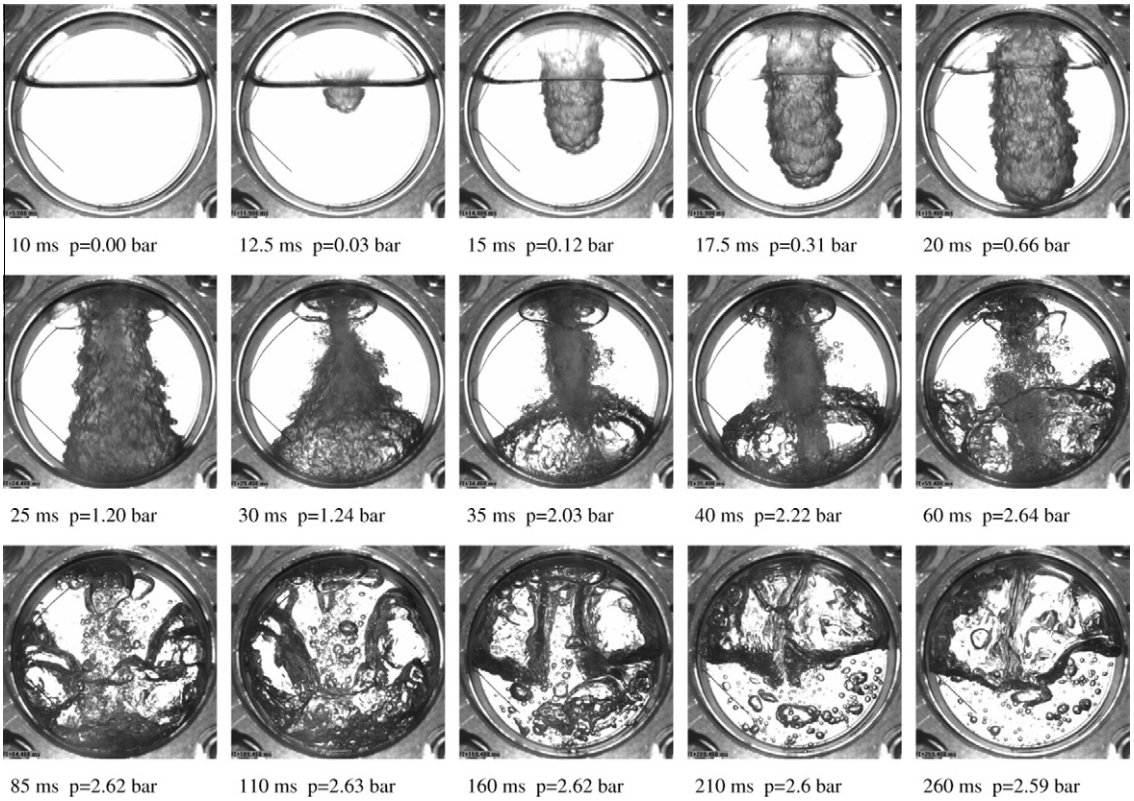

Fig. 11. High speed images of the cold gaseous nitrogen injection into water (run 6). Time from injection trigger signal, and vessel pressure are given below each image.

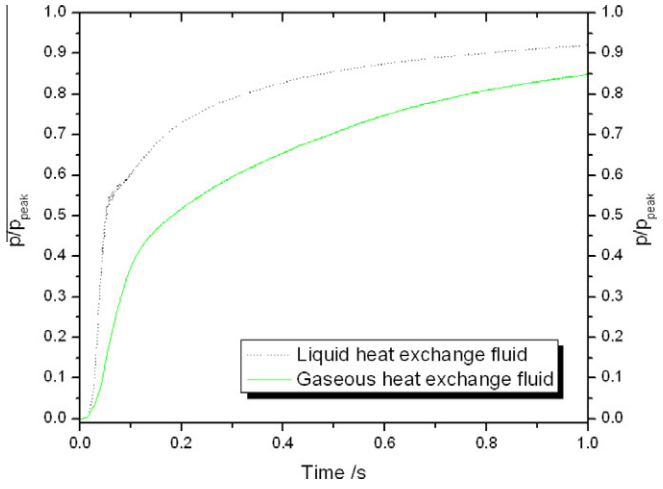

Fig. 12. Liquid nitrogen injection into a liquid (water) and gaseous (air) heat exchange fluid. Pressure shown as a ratio to peak pressure.

Here the subscripts denote an interaction between the systems, and superscripts 1 and 2 the time points before and after the injection respectively. The heat transfer between system A and the apparatus is shown under the term of Q_{other}, whereas the heat transfers between systems B and C and the experimental apparatus is not included in Eq. (2) due to the low temperature difference. For the same reason, the heat transfer between water and ambient nitrogen in the vessel can be neglected, i.e. $Q_{C-B} = 0$. As water is virtually incompressible, the work W_{A-C} and W_{B-C} becomes negligible. With such simplifications, the energy balance of the system can be expressed in terms of the internal energies of each constituent, Eq. (3), which are readily available from property tables for known temperatures.

$$Q_{other} = (U_A^2 - U_A^1) + (U_B^2 - U_B^1) + (U_C^2 - U_C^1) \quad (3)$$

The relative heat distribution among different systems can be estimated if the work W_{A-B} is known. Considering the small temperature change of the nitrogen in the apparatus before and after injection, the work, W_{A-B}, can be estimated by considering an isothermal compression process, i.e. compressing the nitrogen gas in the vessel prior to injection to the peak pressure post injection where experimental data are available. Applied to experimental run 3, this analysis shows that the total heat transfer to the injected nitrogen is 224 J, of which about 82% is from the water, and 5% from the ambient temperature nitrogen in the vessel prior to injection. The remaining 13% (29 J) is the energy conducted to the nitrogen flow by the apparatus, which is predominately from the vessel walls when the nitrogen jet impinges upon them plus a small portion from the nozzle during the injection. Of all the experimental runs for liquid nitrogen injection into water, the average value for Q_{other} is estimated as ~19% with a standard deviation of 14%.

In addition, estimation of the heat transfer with the vessel walls is also undertaken with some empirical correlations, for instance the one proposed by Liu and Wang (2001) Eq. (4). This equation was found to give good results for the boiling of an impinging water jet on a stainless steel plate.

$$Nu_D = 2Re_D^{1/2} Pr^{1/6} \left[\frac{k_v}{k_l} \frac{\Delta T_{sub}}{\Delta T_{sat}}\right]^{1/2} \quad (4)$$

Here, Nu_D and Re_D are the Nussel number and Reynolds number with jet diameter as the characteristic length, k_v and k_l are the thermal conductivity of the gaseous and liquid phase, and ΔT_{sub} ΔT_{sat} represents the initial jet subcooling and superheat at saturation condition. The jet entry conditions for experimental run 3 are estimated using the average mass flow rate and vessel pressure during injection, which gives a jet velocity of ~20 m/s. Based on Eq. (4)

and an approximate contact area, the heat transfer from a pure liquid nitrogen jet impingement onto the wall is estimated as ~32 J. While this figure is remarkably similar to the 29 J calculated through the energy balance above, it should be noted that the correlation makes no account for the separation of nozzle and plate or interaction with an ambient fluid.

It should be emphasised that these simple analysis only gives a rough idea of energy distribution under very simplified assumptions. Detailed calculation requires accurate control of liquid nitrogen injection mass, fully determined thermodynamic status prior and post injection, known jet dynamics and instability under hydrodynamic and thermal imbalance conditions, as well as accurate determination of the liquid temperature profile to know internal energy change in the liquid phase. Detailed modelling based on the computational fluid dynamic (CFD) approach is currently ongoing.

3.4. Implications on the performance of a cryogenic engine

The experimental conditions in this study have been designed to simulate as closely as possible those of a cryogenic engine. However there are some discrepancies in the volumetric and time scales involved. The dead volume within the engine cylinder is of the order of 15 ml, a tenth of that used here. This must also accommodate enough heat exchange fluid to maintain a near atmospheric final temperature. While it is clear that high cylinder pressures can be attained, it is less clear whether they can be reached rapidly enough. Extrapolating for the smaller volume, we might expect a 10-fold increase in pressure and rate of pressure rise. Taking data from run 3, this would result in 1500 bar pressure at a rate of 1750 bar/s. A realistic injection time period may be about 10 ms, the first 36° of an expansion stroke at 600 rpm engine speed. This would allow a peak pressure of 17.5 bar, and an isothermal specific work output of 243 kJ/kg of liquid nitrogen. Unfortunately this does not account for energy expended in injecting the nitrogen into the cylinder at this rate, the high pressures needed to do so, and frictional losses. It is also likely that the rate of pressurisation will not increase monotonically with injection pressure past a certain point. Above this pressure the relation of nozzle flow velocity with pressure will be dominated by cavitation and choking effects and the rate of heat transfer may be limited by fluid properties. The pressure at which this maximum is reached is above the injection pressures tested here, but is certain to be below the 1500 bar used in the example above.

Maximum pressurisation rate is not the only consideration for injections in a cryogen engine: efficient use of all available energy is perhaps more important given the low energy density of nitrogen as a fuel. A significant feature of gaseous injections compared to liquid injections is the attainment of maximum pressure in a shorter time period, albeit a much lower maximum. Total pressure rise time is typically of the order of 100 ms for gaseous injection, compared with 5 s for liquid injections. On this basis it would not be possible to fully expand nitrogen in an engine cylinder if it were injected in liquid form. Either heat transfer during and immediately following injection must be increased dramatically or the load of heat transfer reduced through injection in the multiphase regime.

Further improvements to the heat transfer rate may be achieved through increasing the mixing and hence interface area of the jet on injection. This may be done using higher feed pressures and different nozzles to produce a fine spray or atomisation. Refinements in the injection conditions could enable further gains in peak pressure to be made by increased subcooling allowing greater mass to be injected more rapidly. The vapour explosion interactions discussed by Archakositt et al. (2004) produced very high pressure time derivatives. If it were possible to create the appropriate conditions to induce such an interaction, this could be very beneficial to pressure time derivatives during and after injection. It may not be possible however, as the propagation of a vapour explosion usually requires a significant mass of cryogen. If the relation between injection pressure and volumetric ratio (of water to nitrogen) remains linear outside the boundaries investigated (by Archakositt et al.) then extrapolation suggests an unfeasibly high pressure of 400 bar would be needed for injection at a volumetric ratio of 10. Alternatively, improving thermo-physical properties of the warment fluid, i.e., choose alternative heat transfer fluids or modify heat transfer properties by some additives, can increase heat transfer process further. For instance, many studies have reported in the last decades that some introduction of nanoparticles could increase the thermal conductivities of the base fluids (Buongiorno et al., 2009; Wen et al., 2009); and some reported big increases in boiling heat transfer (Wen et al., 2006b; Park and Jung, 2007). If properly engineered, such a fluid can be introduced that improve the cryogen injection process further. Currently such work is ongoing. In addition, heat transfer with the engine cylinder could be improved. Although heat exchange with the vessel is relatively minor compared to that of the liquid–liquid interaction in these experiments, for the smaller confines of an engine cylinder, this mode of heat transfer may be more significant. Modifications such as internal fins in the cylinder head could therefore be beneficial.

4. Conclusions

A fundamental study of liquid nitrogen injection into water is conducted in this work. A proper design of the experiment allows controlled injection of nitrogen at different thermodynamic states to be established, and the evolution of jet structure to be visualised with synchronized pressure and temperature measurement. A number of interesting phenomena are observed that can be summarized as:

- A four-stage evolution of jet structure is established for liquid nitrogen injection into water through the visualization study, and characterised by different pressurisation rates.
- The largest pressure time derivative occurs during the injection stage (3) in which the structure of the nitrogen jet is stable, with a thick vapour blanket separating its liquid phase and the surrounding water. Jet break-up is primarily a result of impact with the confining walls of the pressure vessel.
- An approximately linear correlation between pressurisation rate in stage (3) and injection pressure is confirmed, and the maximum pressurisation rate of 367 bar/s is recorded at an injection pressure of 14 bar.
- The liquid nitrogen–water injection (L–L) results are compared with other injection experiments, including gaseous nitrogen injection into water (G–L) and liquid nitrogen injection into ambient air (L–G), which allows the contributions of pressurisation from mass transfer, latent heat transfer and sensible heat transfer to be differentiated.
- The benefits of latent heat transfer of liquid nitrogen and the use of water as the heat transfer fluid are characterised, which are affected significantly by the jet structure, especially the interface area of direct contact between liquid nitrogen and the warmant fluid.
- The implication of current experimental result on the performance of a cryogenic engine is illustrated, and future work is identified where a focus will be on the modelling of jet dynamics to form a deeper mechanistic understanding.

Acknowledgements

The authors are grateful for the financial support of EPSRC through a CASE studentship, and Highview Energy Storage Ltd.

References

Archakositt, U., Nilsuwankosit, S., Sumitra, T., 2004. Effect of volumetric ratio and injection pressure on water–liquid nitrogen interaction. J. Nucl. Sci. Technol. 41 (4), 432–439.

Buongiorno, J., Venerus, D., Prabhat, N., McKrell, T., 2009. A benchmark study on the thermal conductivity of nanofluids. J. Appl. Phys. 106, 094312-1–094312-14.

Clarke, H., Crookes, R., Wen, D.S., Dearman, P., Aryes, M., 2009. Development of a Liquid Nitrogen Fuelled Cryogenic Engine. In: TAE 7th International Colloquium Fuels, pp. 649–656.

Dahlsveen, J., Kristoffersen, R., Saetran, L., 2001. Jet mixing of cryogen and water. In: 2nd International Symposium Turbulence and Shear Flow Phenomena, vol. 2, pp. 329–334.

Dinh, T.N., Bui, V.A., Nourgaliev, R.R., Green, J.A., Sehgal, B.R., 1998. Experimental and analytical studies of melt jet–coolant interactions: a synthesis. Nucl. Eng. Des. 189, 299–327.

Duckworth, R.C., Murphy, J.G., Utschig, T.T., Corradini, M.L., Merrill, B.J., Moore, R.L., 2000. Analysis of Liquid Cryogen–Water Experiments with the MELCOR Code. 14th Topical Meeting on the Technology of Fusion Energy.

Harstad, K., 1992. Cryogenic jet mixing model. Heat Transfer Phase Change, p. 205.

Khabeev, N.S., 1999. Simulation of vapour explosions. Appl. Energy 64, 317–321.

Liu, Z.H., Wang, J., 2001. Study on film boiling heat transfer for water jet impinging on high temperature flat plate. Int. J. Heat Mass Transfer 44, 2475–2481.

Nourgaliev, P.R., Dihn, T.N., Haraldsson, H.O., Sehgal, B.R., 2003. A multiphase eulerian–langranian transport (MELT-3D) approach for modelling of multiphase mixing in fragmentation processes. Prog. Nucl. Energy 42 (2), 123–157.

Ordonez, C.A., Plummer, M.C., Reidy, R.F., 2001. Cryogenic heat engines for powering zero emission vehicles. ASME IMEC, PID-25620.

Park, K.J., Jung, D., 2007. Enhancement of nucleate boiling heat transfer using carbon nanotubes. Int. J. Heat Mass Transf. 50, 4499–4502.

Reinke, P., Yadigaroglu, G., 2001. Explosive vaporization of superheated liquids by boiling fronts. Int. J. Multiphas. Flow 27, 1487–1516.

Wen, D.S., Chen, H.S., Ding, Y.L., Dearman, P., 2006a. Liquid nitrogen injection into water: pressure build-up and heat transfer. Cryogenics 46, 740–748.

Wen, D.S., Ding, Y.L., Williams, R., 2006b. Pool boiling heat transfer of aqueous based TiO_2 nanofluids. J. Enhanc. Heat Transf. 13, 231–244.

Wen, D.S., Lin, G., Vafaei, S., Zhang, K., 2009. Review of nanofluids for heat transfer applications. J. Particuology 7 (2), 141–150.